

Toward the Discovery of Functional Transthyretin Amyloid Inhibitors: Application of Virtual Screening Methods

Carlos J. V. Simões,^{†,‡} Trishna Mukherjee,[†] Rui M. M. Brito,[‡] and Richard M. Jackson*,[†]

Institute of Molecular and Cellular Biology, Faculty of Biological Sciences, University of Leeds, Leeds LS2 9JT, United Kingdom and Center for Neuroscience and Cell Biology and Chemistry Department, University of Coimbra, 3004-535 Coimbra, Portugal

Received June 29, 2010

Inhibition of amyloid fibril formation by stabilization of the native form of the protein transthyretin (TTR) is a viable approach for the treatment of familial amyloid polyneuropathy that has been gaining momentum in the field of amyloid research. The TTR stabilizer molecules discovered to date have shown efficacy at inhibiting fibrilization in vitro but display impairing issues of solubility, affinity for TTR in the blood plasma and/or adverse effects. In this study we present a benchmark of four protein- and ligand-based virtual screening (VS) methods for identifying novel TTR stabilizers: (i) two-dimensional (2D) similarity searches with chemical hashed, pharmacophore, and UNITY fingerprints, (ii) 3D searches based on shape, chemical, and electrostatic similarity, (iii) LigMatch, a new ligand-based method which uses multiple templates and combines 3D geometric hashing with a 2D preselection process, and (iv) molecular docking to consensus X-ray crystal structures of TTR. We illustrate the potential of the best-performing VS protocols to retrieve promising new leads by ranking a tailored library of 2.3 million commercially available compounds. Our predictions show that the top-scoring molecules possess distinctive features from the known TTR binders, holding better solubility, fraction of halogen atoms, and binding affinity profiles. To the best of our knowledge, this is the first attempt to rationalize the utilization of a large battery of in silico screening techniques toward the identification of a new generation of TTR amyloid inhibitors.

INTRODUCTION

Amyloid diseases embody a wide spectrum of acquired, inherited, or infectious pathologies that includes diseases, such as Alzheimer's disease, type 2 diabetes, familial amyloid polyneuropathy (FAP), or cardiomyopathy (FAC), and several others with significant socio-economic impact. The formation of amyloid aggregates and fibrils may be seen as a product of deviant protein–protein interactions between conformational intermediates found along the unfolding pathways of certain proteins, and several reports have shown that small molecules can modify the kinetics of fibril formation.¹

Transthyretin (TTR) is a homotetrameric protein present in the blood plasma and cerebral spinal fluid, implicated in the deposition of fibrils in peripheral nerves and heart tissue in FAP and FAC, respectively. This process involves an initial step whereby the native TTR tetramer dissociates to monomers with altered tertiary structure, followed by the self-assembly of these monomers to form cytotoxic oligomers.^{2,3} The initial step was shown to be rate limiting for amyloid formation and can be modulated by the binding of thyroxine-like compounds to the two equivalent and funnel-shaped thyroxine-binding pockets of tetrameric TTR (Figure 1A).^{4–7} Initial limited screenings have shown that nonsteroidal anti-inflammatory drugs (NSAIDs) can bind TTR with high affinity, stabilize the tetramer, and thereby prevent amyloid

formation in vitro.^{8–10} Over the past decade, several analogues and derivatives have been discovered and designed, showing potential as drug candidates.^{4,11–19} Fragment-based approaches are being followed to identify the most efficient combinations for the substructural elements composing the classic binder.^{20–22} More recently, a new family of designed stilbenes that covalently modify TTR has been presented.²³ Although several stabilizer molecules discovered to date have shown efficacy at inhibiting fibrilization in vitro, the optimal balance between affinity and selectivity for TTR in the blood plasma is still a goal to achieve. Furthermore, the NSAID-derived scaffold (comprised of two aromatic rings typically substituted with halogens) is associated with undesirable properties, such as poor solubility and low polar surface areas, which are in turn linked with important adverse effects and accumulation in the body.

With the ever-growing availability of detailed three-dimensional (3D) structures of target proteins determined by X-ray crystallography and nuclear magnetic resonance (NMR), the design of highly selective drugs should become tractable. However, in numerous cases this task has proved nontrivial. Although establishing complementary interactions with the target receptor, the designed compounds may display undesirable absorption, distribution, metabolism, excretion, and toxicity (ADMET) properties, as a consequence of a high molecular weight or highly reactive groups. Moreover, although therapeutically relevant, the target receptors may lack selective deep pockets or grooves required for the high-affinity binding of small molecules. In such cases, the binding

* Corresponding author. E-mail: r.m.jackson@leeds.ac.uk. Telephone: +44 (0)113 343 2592.

[†] University of Leeds.

[‡] University of Coimbra.

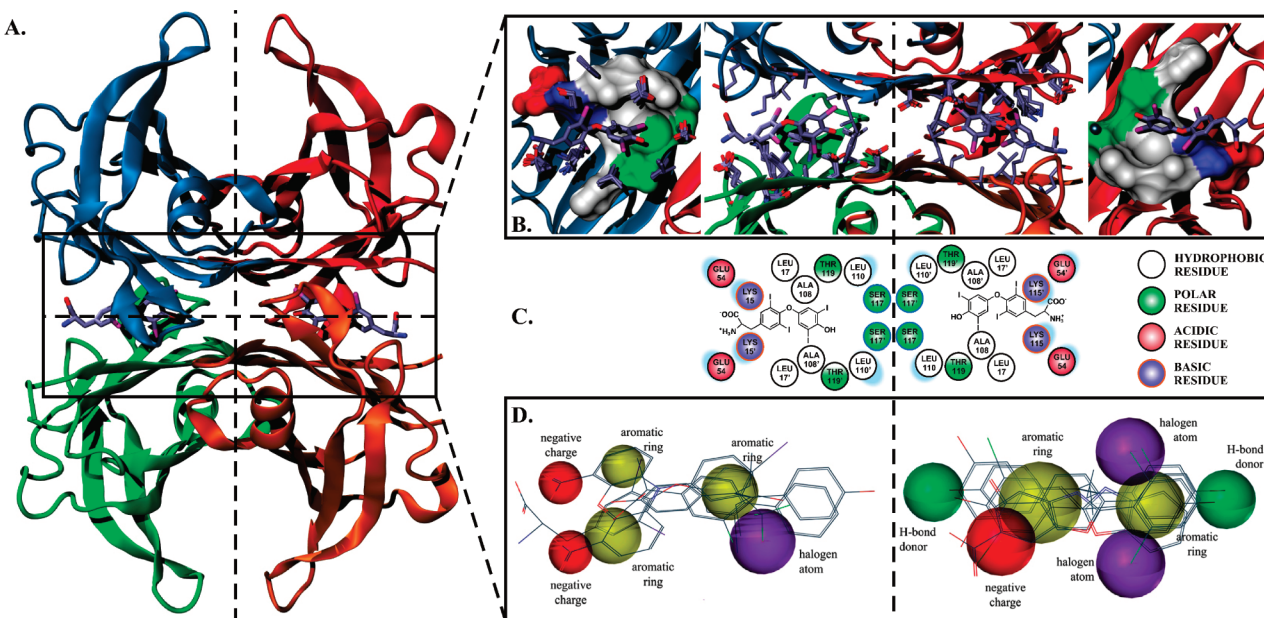


Figure 1. (A) Three-dimensional (3D) ribbon representation of the X-ray crystallographic structure of homotetrameric WT-TTR (PDB code 2rox), with thyroxine (T_4) bound within the two symmetrical binding sites created at the dimer–dimer interface (horizontal dashed line). Each color represents one of the four TTR monomers. (B) Expanded views of the two pockets from two different perspectives. In the central panels, the result of a multiple structural alignment of 28 TTR complexes is displayed as licorice drawings for the side chains of one of the monomers in the binding site. At the edge panels, the molecular surface of binding site residues is shown. At the rightmost panel, a conserved water molecule bridging the adjacent Ser-117 and Ser-117' hydroxyl side chains is shown as a blue bead. (C) 2D topology diagram with a graphical legend of binding site features. (D) 3D pharmacophore hypothesis generated for TTR receptor sites. The two hypotheses shown are based on two different clusters obtained from analysis of 3D structures of complexes of TTR with known TTR amyloid inhibitors (HYP AC1 on the left and HYP BD1 on the right). The most important binders of each cluster are represented.

of small organic molecules to these sites is usually driven by nonspecific hydrophobic and van der Waals interactions, and the corresponding targets are often regarded as “high risk”, “undruggable”, or even “promiscuous”, as some researchers may regard TTR.²⁴

From the viewpoint of the design of organic molecules to interfere with amyloid formation, TTR is both an appealing target and a challenging one. The availability of structural data of TTR bound to a number of ligands is extensive, with more than 60 complexes of human TTR at 2 Å resolution or better deposited in the Protein Data Bank (PDB). This strongly encourages the exploitation of structure-based virtual screening (VS) methods like molecular docking and receptor-site pharmacophore models to identify compounds establishing optimal interactions within the receptor sites of TTR. However, binding sites mainly comprised of nonpolar residues and lacking an adequate number and/or placement of hydrogen-bonding groups or other specific pharmacophore features are frequently associated with poor predictions of binding affinities by docking scoring functions.²⁵ Ligand-based VS approaches, such as 2D fingerprint similarity,^{26,27} 3D shape-matching,²⁸ or 3D pharmacophore searches²⁹ have provided good results, outperforming molecular docking,³⁰ and may be valuable for identifying compounds with appropriate shape, chemical topology, and electrostatic properties similar to those of the reference TTR stabilizers and with better affinities and/or ADMET profiles. Indeed, the elucidation and characterization of novel, structurally diverse and selective binders may also shed light on some of the idiosyncrasies surrounding ligand binding to TTR that remain poorly understood: Firstly, the negative cooperativity observed for some of the known binders seems to be more related to electrostatic interactions between two binders than

to conformational changes brought about by binding of the first ligand³¹ and, secondly, its propensity to bind biphenyls and molecules bearing multiple halogen atoms.

In this study we test and compare the performance of four different VS methods for identifying active TTR stabilizer compounds seeded in a set of 738 carefully selected decoys. Among the studied VS methods are: (i) 2D similarity searches using both chemical hashed and pharmacophore fingerprints with ScreenMD³² and UNITY 2D fingerprints with SYBYL,³³ (ii) 3D searches based on shape, chemical, and electrostatic similarity using ROCS³⁴ and EON,³⁵ (iii) a new ligand-based method combining 2D preselection from multiple templates with 3D geometric hashing called Lig-Match,³⁶ and (iv) molecular docking with AutoDock 4³⁷ and FRED³⁸ into consensus TTR X-ray structures selected by cross-docking studies. Moreover, we disclose the results of the best-performing protocols on a tailored library of approximately 2.3 million drug-like compounds. The top-scoring compounds are evaluated in terms of their molecular properties, predicted binding affinities, and compliance with 3D pharmacophore models devised to differentiate the distinct binding modes observed for some of the known binders on each TTR pocket.

METHODS

X-ray Model Evaluation. Twenty-eight TTR high-resolution X-ray complexes were selected following structural quality evaluation with WHAT IF³⁹ and PROCHECK.⁴⁰ Because the asymmetric unit of all orthorhombic crystal lattices only accounts for the structure of one TTR dimer, the respective full biological unit of each complex was obtained from the protein quaternary structure server.⁴¹ All

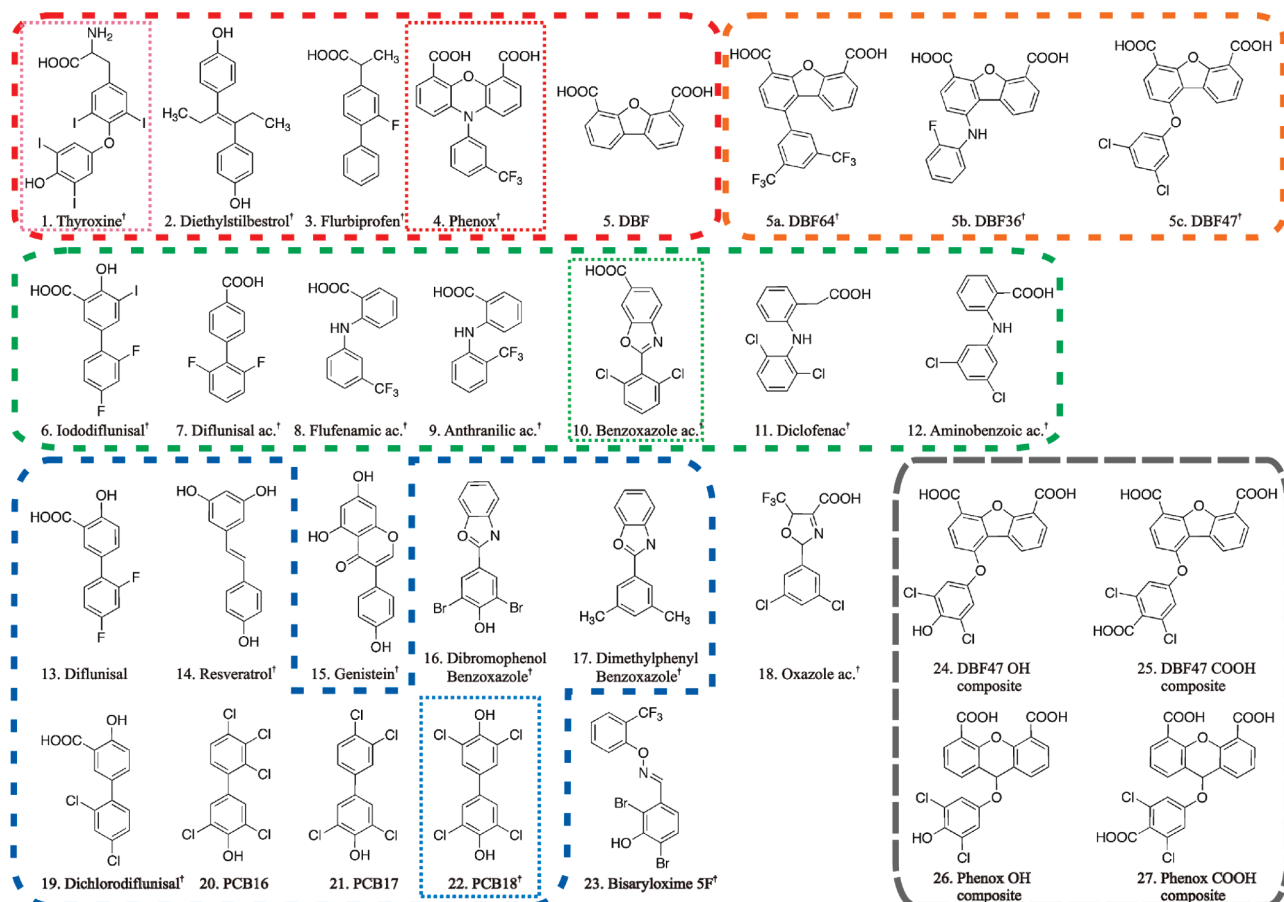


Figure 2. TTR binders reported in the literature and/or deposited in the PDB and modeled composite ligands. Ligand mapping following an overlay of multiple TTR complexes revealed three clusters of ligands occupying similar geometrical positions within TTR binding pocket AC: red, green, and blue (clusters A, B, and C, respectively) dashed boxes. These three groups were used for the generation of UNITY 3D pharmacophore models for pocket AC of TTR. The orange dashed box comprises molecules from three classes of dibenzofuran-based inhibitors: compound 5c has the highest efficiency inhibiting fibril formation, compound 5b shows the highest plasma binding stoichiometry, and compound 5a represents a compromise between inhibition of fibril formation and binding stoichiometry.¹⁹ Compounds highlighted by the dotted boxes were used as template queries for 2D and 3D similarity searches in this work. The gray dashed box comprises four composite ligands that were modeled using compounds 4 and 5c as reference. Ligands marked with a † were used as actives in the test set.

complexes were aligned using a geometric hashing algorithm⁴² on an all-against-all basis, and similarity scores were computed by comparison of C_{α} atom coordinates. Then, all complexes were aligned onto the complex holding the highest overall structural similarity, the structure of TTR bound to 4-hydroxy-2',3,3',4',5-pentachlorobiphenyl (PDB accession code 2g9k). Ligand structures of all complexes were verified visually to ensure that no atom–atom clashes were present. A calculation of conformational energies was performed (using the MMFF94 force-field)⁴³ to ensure that no ligand structures had high strain energies.

3D Pharmacophore Modeling. Twenty aligned protein–ligand complexes described in the previous section were used to define training sets for the modeling of 3D pharmacophore hypotheses (HYP). Ligand mapping was initially performed by means of an all-atom comparison of ligand atom coordinates resulting from the superimposition of the 20 complexes. Coordinates found to be identical or lying within 1 Å distance in two bound ligands were considered a “hit”, and the total number of hits was computed and used to calculate pair wise Tanimoto indexes for all ligands on each of the two TTR pockets. The resulting similarity score matrix was clustered and produced three underlying groups of ligands (the training sets) occupying similar geometrical

positions within TTR binding pocket AC (see Figure 2) and two groups within pocket BD. The ligand mapping procedure was performed using a java script written in-house, and the clustering was carried out with CLUTO.⁴⁴ Each training set was translated into ligand-based 3D pharmacophore queries using SYBYL and UNITY³³ (see Figure 1D). Receptor information was then used to add exclusion volume spheres to the models and thus define the shape of the TTR binding pockets. More detailed information on pharmacophore modeling procedures is provided in the Supporting Information.

Test Set. To evaluate the discriminative power of different virtual screening methods, we compiled a test set of active and inactive compounds. Initially, we collected information on known TTR binders reported in the literature and deposited in the PDB.^{4,11–19} On this basis, 22 binders were then selected as “actives” making use of the available binding affinity data and clustering by maximum common substructure³² to ensure maximal diversity and therefore to avoid the inclusion of compounds coming from the same series. The selection of inactive compounds (decoys) for use in the evaluation of VS protocols is of critical importance, as we seek to evaluate the algorithms’ power to discriminate actives over inactives based on the compounds’ ability to establishing complementary interactions within the receptor site rather

than by inconsequential physicochemical properties, such as their molecular weight. To select our decoys we followed a strategy similar to the one used to build the Directory of Useful Decoys (DUD).⁴⁵ This involved three main steps, starting with a library of 5 million Lipinski-compliant molecules deposited in the ZINC database of commercially available compounds.⁴⁶ 2D dissimilarity analysis was performed by using UNITY fingerprints³³ and by computing Tanimoto similarity coefficients between each active and every compound in the library. Compounds holding a Tanimoto coefficient of greater than or equal to a threshold of 0.5 to any of the annotated actives were excluded, and the initial library was thus reduced to approximately 4.5 million compounds topologically dissimilar to the TTR binders. Second, for each active ligand we extracted from the library approximately 100 ZINC compounds possessing similar physical properties. This was carried out by using the program FILTER⁴⁷ and by defining narrow property ranges for the numbers of heavy atoms, hydrogen-bond donors and acceptors, and rotatable bonds and the sum of formal charges and octanol/water partition coefficient (XlogP). Finally, we performed diversity (clustering) analysis by computing 2D similarity within each group of 100 ZINC compounds and thus selecting representatives holding highest dissimilarity. This ensures that, as far as possible, each decoy is representative of a unique chemical series when considered by the VS algorithms. After removing all redundant entries from an initial set of 786 compounds, a final set of 738 decoys was obtained (approximately 34 decoys per active). The annotated actives were then seeded among these 738 decoys to constitute the final validation test set.

Screening Set. To assess the potential of the different methods on a pilot large-scale VS campaign for identifying novel TTR stabilizers, a tailored library of 2 259 573 compounds was created by filtering an initial database of approximately 11 million molecules deposited in ZINC.⁴⁶ The filtering consisted of a combination of predefined rules for drug-likeness and bioavailability with knowledge of the physicochemical properties of the known TTR stabilizers. The predefined rules included Lipinski's rule-of-five,⁴⁸ allowing up to two violations and defining hydrogen-bond donors and acceptors, as outlined in the work of Mills and Dean,⁴⁹ Veber's (GSK) rules,⁵⁰ Martin's (Abbott) bioavailability score,⁵¹ and Pharmacopia's "Egan egg" bioavailability rule.⁵² We also filtered out aggregators and predicted aggregators, i.e., small molecules known or predicted to aggregate and sequester protein in solution, thus interfering with assay results.^{53,54} Molecules predicted to be insoluble or poorly soluble in water were discarded as well. Furthermore, based on the distribution of various physicochemical properties for the known TTR actives, we applied filter definitions to ensure that no redundant molecules were included and that no potential binders were missed at an early stage of the virtual screening. Thus, the maximum halide fraction (percent of molecular weight from halides) was increased to 0.6, the maximum sum of formal charges decreased to 0, the maximum XlogP increased to 6.5, and iodine was added to the list of allowed elements. All filtering procedures were performed with FILTER.⁴⁷

Conformer Generation. Multiple ligand conformations (conformers) were generated for all ligands in the test and screening sets using Openeye's OMEGA.^{55,56} A maximum

of 100 conformers were generated per molecule with a diversity threshold of 1 Å root-mean-square deviation (rmsd) to discard similar conformations. These parameters represent an optimal balance between speed and performance.⁵⁷ Moreover, an energy window of 25 kcal·mol⁻¹ was used since it was proven critical for best conformer generation performance.⁵⁷ A lower energy window could cause valuable conformations to be discarded, whereas a higher energy threshold could produce high-energy conformers unlikely to represent bioactive conformations.

Template Ligands for Ligand-Based Virtual Screening.

The choice of the active molecules to use as a reference query for both 2D and 3D similarity searches is a critical issue. First, it is very unlikely that one single active molecule can be representative of a whole series of actives or even hold all the ideal pharmacophoric features required for optimal interaction with the target binding site. Moreover, 3D similarity search methods would ideally take the bioactive conformation of the reference ligand as a query for the searches, but sometimes this is unavailable.

For the comparison of the different similarity-based VS methods described in the following subsections, we chose the cognate ligand, thyroxine (compound **1**, see Figure 2),⁵⁸ the most prominent endogenous TTR binder; phenoxy (compound **4**),¹² a promising TTR stabilizer and representative of cluster A; a benzoxazole acid (compound **10**),¹⁵ another potent amyloid inhibitor representative of cluster B; and a polychlorinated biphenyl (compound **22**),¹⁶ the most potent TTR binder known so far and representative of cluster C (Figure 2). In all cases, the structures of the template ligands were extracted from the corresponding X-ray coordinates deposited in the PDB: 2rox for thyroxine (**T₄**), 1dvy for phenoxy, 2f8i for the benzoxazole acid, and 2g5u for the polychlorinated biphenyl (PCB18). DBF47 (compound **5c**) is a potent dibenzofuran derivative sharing structural similarity with phenoxy.¹⁹ Because no X-ray coordinates are publicly available for the full structure of DBF47 (compound **5c**), we took the coordinates of the dibenzofuran-4,6-dicarboxylic acid moiety (compound **5**) in the complex with TTR (PDB code 1dvu) and modeled in the missing 3,5-dichloro aryl ether substituent.

To address the aforementioned problem of "representativeness" among the training sets, we took the structures of both compounds **4** and **5c** and modeled in missing features that are believed to be critical for both shape complementarity with the receptor sites of TTR and interaction with the hydroxyl side chains of two serine residues located at the inner portion of the pockets.^{12,13,17} This resulted in four new composite ligands that are concatamers of these high-affinity ligands. Two ligands (compounds **24** and **25**) were based on the structure of DBF47 (compound **5c**), and the other two (compounds **26** and **27**) were based on the structure of compound **4**. X-ray coordinates were used as a template (PDB code 1dvy), and the hydroxyl and carboxyl groups were added at the para position of the distal aryl ring. Since the trifluoromethyl group at the meta position of this ring is rather bulky to favorably allow the presence of a substituent at the para position, we replaced it with a chlorine atom and added an extra chlorine at position 5 (creating symmetry). This modification was inspired by the successful substitution pattern of the corresponding ring in DBF47.¹⁹ The composite structures were then energy minimized, and conformational

sampling was performed to identify low-energy conformations retaining the closest similarity to the X-ray reference models. All modeling procedures were carried out with ChemAxon's MarvinSketch.⁵⁹ Conformational sampling was performed with OMEGA. The predicted lowest-energy conformations were evaluated as potential template queries for VS.

Chemical Hashed Fingerprints, 2D Pharmacophore and 2D UNITY Fingerprints: 2D Similarity Searching.

Chemical hashed (CHF) and 2D pharmacophore (2D-PF) fingerprints were generated for all ligands in the test and the screening sets using ChemAxon's GenerateMD. Then, ScreenMD was used to evaluate the performance of these two descriptors with two different measures of similarity (the Euclidean distance and the Tanimoto coefficient) on the test set. Both GenerateMD and ScreenMD are part of ChemAxon's JChem package.³² Equally, UNITY was used within SYBYL³³ to generate 2D standard screens (UNITY 2D fingerprints) and to perform 2D similarity searches on the test and screening sets. All templates, including the composite ligands, were used individually both for evaluation and screening purposes. A more detailed description of the 2D fingerprints tested here is provided in the Supporting Information.

3D Shape and Chemical Similarity Searches. Electrostatic Similarity Searches. 3D-similarity searches were performed using ROCS³⁴ and EON.³⁵ ROCS is a shape-based method that assesses the volume overlap of two molecules, using Gaussians parametrized according to the hard-sphere volume of heavy atoms.²⁸ Upon superposition this method evaluates molecular similarity according to shape and chemistry definitions after alignment of multiple conformers of a target molecule to a template query. The ROCS combo score is the sum of two measures of similarity: the shape Tanimoto and the scaled color score; the former being a measure of the shape similarity, and the latter being a measure of the chemical match between two molecules. Here we used both the ROCS combo and the scaled color scores to rank the test and screening sets against all template ligands.

Electrostatics plays an important role in the binding of ligands to TTR.³¹ Analyses of the electrostatic potential have shown that the surface potential is more positive in the two binding sites than in other regions of the protein surface, due to the influence of the ammonium groups of two Lys-15 residues.^{60,61} In addition, the median of the sum of formal charges for the 22 active ligands selected for the test set is -1, disclosing a tendency to bind negatively charged molecules. This is also in agreement with TTR's well-known propensity to bind halogen-bearing (electronegative) molecules. It is therefore tempting to search for small molecules holding electrostatic properties similar to the template ligands. The program EON takes the molecular overlays produced by ROCS as input and a field-based measure of Tanimoto to compare the electrostatic potential of a target molecule with a template molecule. EON then outputs two different electrostatic Tanimoto measures and an electrostatic Tanimoto combo (ET combo), which is a sum of the shape Tanimoto and the Poisson–Boltzmann electrostatic Tanimoto. We used the ET combo to evaluate the performance of EON on the test set and to rank the entire screening set.

LigMatch: 3D Geometric Matching Upon 2D Selection from Multiple Templates. Given the considerable structural diversity of the known TTR binders, it seems clear that no single template can entirely represent a global pharmacophore

for binding to TTR. In this work we explore a recent method that combines 2D preselection from multiple templates with 3D geometric hashing.³⁶ In the first step, LigMatch uses a 2D fingerprint-based method to calculate Tanimoto coefficients between each molecule in a database to be screened and each of the available template ligands. Then, following the MAX fusion rule, the 3D ligand template with the highest Tanimoto coefficient is selected as the template against which all the conformers of that molecule are aligned to and scored using a geometric hashing algorithm.⁴² Finally, the compounds are ranked according to a normalized mean 3D similarity score. If only one template is available, then the 2D selection step is skipped (single template mode or STM for short).

In this work, the atom–atom score was determined for every conformer of every molecule in the test and screening sets, and each molecule was assigned both a best (conformer) and a mean atom–atom score (based on all conformers). To deal with the maximum possible number of matching atoms, these were then normalized by dividing by the number of atoms present in that given molecule. The resulting lists were then ranked by both the descending normalized best and mean scores. To allow the direct comparison of the performance of LigMatch with the other similarity search methods introduced above, we used the same X-ray templates to perform the searches over the test set.

Structure-Based Virtual Screening: Docking and Scoring Validation. Redocking of the cocrystallized ligands into its respective TTR receptor was performed using AutoDock 4 (AD4) version 4.01,³⁷ eHiTS version 6.2,⁶² GOLD version 3.2,⁶³ and FRED version 2.2.³⁸ AD4 and GOLD employ stochastic search algorithms for sampling ligand conformations, whereas eHiTS and FRED perform systematic searches to find ligand poses within the binding sites. Docking poses generated by AD4 and eHiTS were scored using the scoring functions implemented as objective functions in the docking algorithms (free energy function for AD4 and eHiTS scoring function for eHiTS). All docking poses generated with GOLD were rescored using GoldScore,⁶³ ChemScore,⁶⁴ and ASP.⁶⁵ All docking poses generated by FRED were rescored using ChemGauss2 and ChemGauss3,³⁸ ChemScore,⁶⁴ PLP,⁶⁶ and ScreenScore,⁶⁷ after pose optimization with ChemGauss3. For each ligand, the top 10 ranked poses were evaluated by comparison with the respective X-ray pose. To take account of symmetry effects, an rmsd score was calculated using a graph isomorphism algorithm.

AutoDock 4 version 4.01 was used for cross-docking with the best 28 TTR complexes previously selected, whereby every X-ray ligand was docked into every X-ray TTR receptor. This study was carried out after randomization of each ligand's initial pose with OMEGA. The ligands of the test set were docked into the three best performing receptor structures using AutoDock 4 versions 4.01 and 4.22 and FRED version 2.2. The lowest-energy ligand poses generated by AD4 were reranked with DrugScore-CSD and -PDB.⁶⁸ All docking poses generated by FRED were rescored and reranked using ChemGauss3, ChemScore, and a Consensus scoring function.³⁸ Finally, all ligands in the screening set were docked with FRED and ranked using ChemGauss3 and ChemScore.

Comparison of Methods: Quantitative Description of Hit Lists. The overall performance of the different VS methods was compared by plotting receiver operating

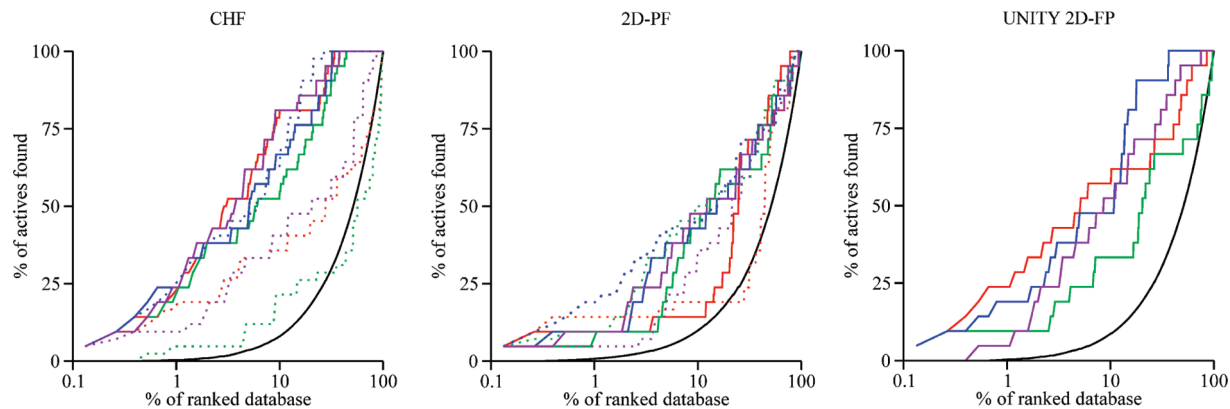


Figure 3. ROC curves to compare the VS performance of three different 2D fingerprint-based methods on a test set created for TTR: ChemAxon chemical hashed (CHF) and 2D pharmacophore (2D-PF) fingerprints and Tripos UNITY 2D fingerprints. For CHF and 2D-PF, the straight lines represent the use of the Euclidean distance as a measure of similarity, whereas the dotted lines represent the use of a Tanimoto coefficient. For UNITY 2D-FP only the Tanimoto coefficient was used. The line colors correspond to different templates as follows: phenox (1dvy) in red, benzoxazole acid (2f8i) in green, PCB18 (2g5u) in blue, and T₄ (2rox) in violet. Random performance is depicted by the black line.

Table 1. ROCE Values at 0.5, 1, 2, and 5% and AUC Values of ROC Plots for the 2D Similarity Methods Tested on TTR^a

method/similarity measure/template		enrichment					ROCE AUC
		0.5% ^b	1%	2%	10%		
chemical hashed fingerprints	Euclidean distance	phenox (1dvy)	142.0	59.5	42.2	16.3	0.92
		benzoxazole (2f8i)	142.0	59.5	42.2	11.0	0.88
		PCB18 (2g5u)	max.	59.5	42.2	12.9	0.90
		thyroxine (2rox)	142.0	59.5	42.2	18.8	0.92
	Tanimoto	phenox (1dvy)	94.8	38.0	13.6	7.9	0.61
		benzoxazole (2f8i)	5.9	5.2	2.6	2.5	0.44
		PCB18 (2g5u)	max.	101.0	42.2	12.9	0.93
		thyroxine (2rox)	47.5	11.9	11.2	7.9	0.70
2D pharmacophore fingerprints	Euclidean distance	phenox (1dvy)	47.5	11.9	5.6	3.0	0.72
		benzoxazole (2f8i)	11.8	11.9	5.6	5.4	0.72
		PCB18 (2g5u)	47.5	11.9	5.6	9.5	0.73
		thyroxine (2rox)	47.5	11.9	8.9	6.6	0.73
	Tanimoto	phenox (1dvy)	142.0	23.7	8.9	3.6	0.58
		benzoxazole (2f8i)	47.5	11.9	9.6	9.5	0.76
		PCB18 (2g5u)	max.	38.0	25.8	11.0	0.76
		thyroxine (2rox)	11.8	5.2	2.6	4.1	0.70
UNITY 2D fingerprints	Tanimoto	phenox (1dvy)	max.	59.5	33.3	12.5	0.80
		benzoxazole (2f8i)	47.5	11.9	5.6	5.3	0.66
		PCB18 (2g5u)	142.0	38.0	18.3	12.5	0.90
		thyroxine (2rox)	11.8	5.2	12.7	9.5	0.83

^a The best combinations of method and template are identified in bold. ^b This percentage of the ranked test set of 760 ligands corresponds to only 4 ligands. When these top-scoring ligands are all actives, the ROCE value becomes the result of a division by zero. Accordingly, the result is presented as “max.”

characteristic (ROC) curves.⁵⁷ Since the enrichment factor (EF) shows dependence on the ratio of actives to decoys in a test set, we used ROC enrichment (ROCE), which expresses the percentage of actives observed as a proportion of the percentage of the decoys observed, not as a proportion of the percentage of the entire test set observed.⁶⁹ Early enrichment is also an important measure of performance in VS, as it is likely that only a small fraction of the screened library of compounds will be subject to experimental evaluation. Therefore, we report ROCE values at 0.5, 1, 2, and 5% of the ranked database. As with the EF, ROCE values greater than 1.0 represent enrichment with respect to random. The area under the ROC curve (AUC) was also calculated, providing a measure of VS performance across the entire

data set. Unlike the EF, the AUC shows no dependence on the ratio of actives to decoys in a database. Ideal distributions of actives and decoys result in an AUC value approaching 1.0, whereas random distributions result in a value of 0.5.

RESULTS AND DISCUSSION

2D Similarity Searches. Figure 3 shows the ROC curves obtained using three 2D fingerprint-based methods and different measures of similarity. ROCE values at 0.5, 1, 2, and 5% of the ranked test set are given in Table 1.

Overall, the enrichment achieved using CHF as molecular descriptors and the Euclidean distance (ED) as the measure of similarity between the test set molecules and the templates

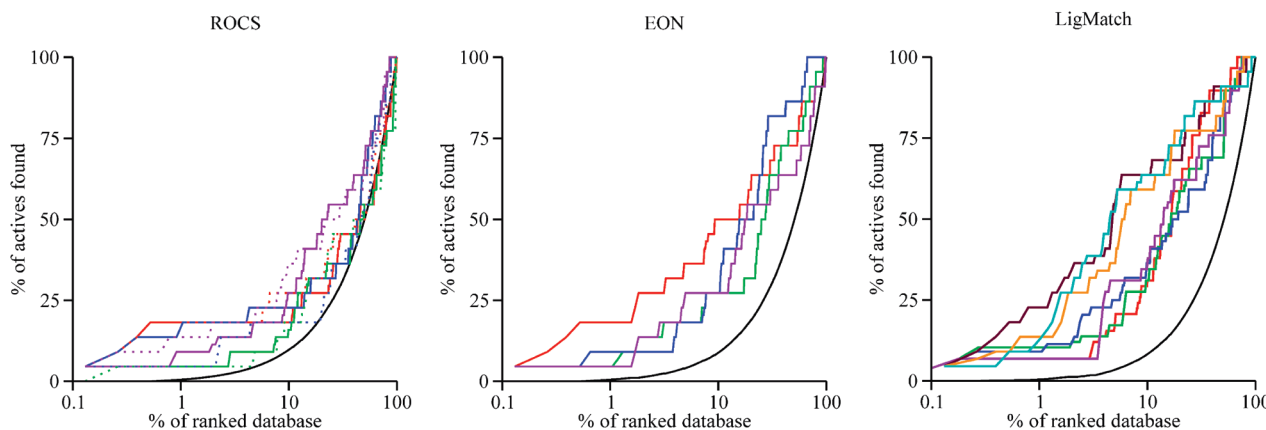


Figure 4. ROC curves to compare the VS performance of different single-template 3D similarity search methods (ROCS, EON, and LigMatch’s single-template mode) on the test set created for TTR. The performance of LigMatch’s multiple-template mode is also illustrated. For ROCS (leftmost panel), the straight lines represent the use of the (default) combo score as a measure of similarity, whereas the dotted lines represent the use of the scaled color measure. The line colors correspond to different templates. For the single-template methods: phenox (1dyv) in red, benzoxazole acid (2f8i) in green, PCB18 (2g5u) in blue, and T₄ (2rox) in violet; and for the multiple-template LigMatch schemes: phenox + benzoxazole acid + PCB18 + T₄ in maroon, phenox + benzoxazole acid + PCB18 in orange, and phenox + PCB18 + T₄ in turquoise.

is the best of all methods explored for TTR. The use of the Tanimoto coefficient with CHF yields poor global enrichments, as disclosed by the low AUC values for most templates. However, the results are highly template dependent in terms of early enrichment. In fact, when using CHF with the Tanimoto metric, the PCB18 template (compound 22) is an outstanding exception, attaining the best results of the whole benchmark when compared to all other X-ray-derived templates. In contrast to CHF, the 2D-PF seems to provide better early enrichment when using the Tanimoto metric as opposed to the ED metric, although similar AUC values are obtained for the two metrics. UNITY 2D fingerprints provide the best results using the Tanimoto coefficient, yielding high early enrichment with the phenox template (compound 4) and high overall enrichment with the PCB18 template. As verified for the CHF descriptors, the PCB18 template seems to hold the highest level of similarity to TTR binders within the 2D descriptor space. This may relate to this compound’s high affinity for TTR.^{16,20}

3D Similarity Searches and LigMatch. The enrichment curves for all single-template 3D similarity search methods are given in Figure 4. For comparison purposes, we tested LigMatch’s single-template mode against each of the available templates. In its multiple-template mode, LigMatch employs a preliminary 2D selection from the available templates prior to the 3D alignment and similarity comparison of the molecules with the templates. We present its results along with those obtained from ROCS and EON to illustrate the benefit of using multiple templates in a single virtual screening run. ROCE values at 0.5, 1, 2, and 5% of the ranked test set, and the area under the ROC curves are given in Table 2.

3D Shape and Chemical Similarity Searches with ROCS. The best overall enrichments for ROCS are obtained with the thyroxine template when using the chemical complementarity descriptor alone (as implemented in the scaled color scoring function), with an AUC of 0.66, and when using the combination of the molecular shape and the chemical complementarity descriptors (as implemented in the combo score function), with an AUC of 0.65. Interestingly, these results seem to agree with the binding charac-

teristics of T₄ to TTR. T₄ (compound 1) presents a more complete set of pharmacophoric features to interact with TTR binding sites (including a hydroxyl group at the inner aromatic ring and a positively charged amino group at the outer tail), but the presence of the four iodine atoms renders it too bulky and hinders its diffusion into the pockets (thus, decreasing its binding affinity). On the other hand, the best early enrichments are attained with the phenox and the PCB18 templates when applying the combo score, yet sharply decreasing beyond the 1% threshold and detecting no more than 25% of the actives at 10% of the ranked database. Holding less bulky halogen atoms and fewer degrees of rotational freedom in their structure, these templates present the shape and the chemical features that better represent the strongest TTR binders, therefore, capturing them at the top of the ranked lists. The results obtained with ROCS reveal poor overall enrichments compared to all other methods tested in this study, which suggests that molecular shape and chemical complementarity are weak descriptors of the diversity of TTR actives.

Electrostatic Similarity Searches with EON. The inclusion of a descriptor of the electrostatic properties of TTR binders was expected to be beneficial, given TTR’s propensity to bind neutral to negatively charged molecules or molecules bearing electronegative elements (halogens). EON takes molecular alignments generated by ROCS and computes a Poisson–Boltzmann ET score between each database molecule and the query template. In Figure 4 and Table 2 we report the results obtained with EON using the ET combo score, which is a sum of the ET and a shape Tanimoto.

Analyzing the differences between EON and ROCS, we observe a slight improvement in terms of overall enrichment, with the PCB18 template showing the highest increase in AUC. In terms of early enrichment, the only considerable improvement occurs for the phenox template, specifically at 2 and 5% of the ranked database (ROCE of 22.7 and 9.1, respectively). It is worth noting that 50% percent of the actives (11 hits) are retrieved within 10% of the top-scored compounds. Indeed, this is the best result obtained with a 3D similarity search method using a single template derived from an X-ray complex. A reasonable decline in early

Table 2. ROCE Values at 0.5, 1, 2, and 5% and AUC Values of ROC Plots for the 3D Similarity Methods and LigMatch^a

		method/similarity measure/template	enrichment				ROCE AUC
			0.5% ^b	1%	2%	10%	
ROCS	scaled color	phenox (1dvy) benzoxazole (2f8i) PCB18 (2g5u) thyroxine (2rox)	max. 11.3 136.0 11.3	36.2 5.0 36.2 11.3	12.9 2.5 12.9 6.9	4.0 1.9 5.2 4.0	0.54 0.51 0.61 0.65
		phenox (1dvy) benzoxazole (2f8i) PCB18 (2g5u) thyroxine (2rox)	max. 11.3 11.3 45.0	36.2 5.0 22.7	12.9 2.5 12.9	4.0 4.0 5.2	0.58 0.51 0.56 0.66
	EON	phenox (1dvy) benzoxazole (2f8i) PCB18 (2g5u) thyroxine (2rox)	max. 11.3 11.3 11.3	36.2 5.0 11.3	22.7 8.5 5.3	9.1 4.0 4.0	0.73 0.68 0.78
		phenox (1dvy) benzoxazole (2f8i) PCB18 (2g5u) thyroxine (2rox)	22.7 51.5 45.0 22.7	8.5 14.7 11.3 8.5	3.8 7.3 6.9 3.8	3.8 3.7 5.7 7.4	0.79 0.74 0.74 0.76
	LigMatch	phenox (1dvy)+ benzoxazole (2f8i) + PCB18 (2g5u) + thyroxine (2rox)	max.	56.8	36.1	15.6	0.84
		phenox (1dvy) + benzoxazole (2f8i) + PCB18 (2g5u)	45.0	22.7	22.7	9.1	0.82
		phenox (1dvy) + PCB18 (2g5u) + thyroxine (2rox)	45.0	23.7	22.7	14.7	0.83

^a The best combinations of method and template(s) are identified in bold. ^b This percentage of the ranked test set of 760 ligands corresponds to only 4 ligands. When these top-score ligands are all actives, the ROCE value becomes the result of a division by zero. Accordingly, the result is presented as “max.”

enrichment is observed for the PCB18 template. This is probably linked to this compound’s peculiar electronegative potential, which is due not only to the presence of four halogen atoms but also to their electron-withdrawing inductive effect over the two hydroxyl groups, rendering them deprotonated and, hence, negatively charged. This distinctive feature seems to separate this template from actives with similar shape, namely compounds **6** and **19** (see Figure 2), causing the loss of early enrichment. However, potent inhibitors from cluster B (compounds **8–10** and **12**) and compounds **3**, **4**, **5b** and **c**, and **23**, which all receive very weak scores by ROCS with the PCB18 template, are placed at much higher levels of the ranked list with EON, explaining the increase in overall enrichment.

Application to Single Templates with LigMatch. The average AUC for the four single templates tested with LigMatch’s single-template mode is 0.76, a result that represents an improvement with respect to EON and ROCS (average AUC of 0.71 and 0.58, respectively) but not with respect to those obtained with the 2D CHF employing the Euclidean distance (average AUC of 0.91). In terms of early enrichment, while other ligand-based methods perform very well with at least one of the templates, LigMatch’s single-template mode offers a more modest/equilibrated performance. Interestingly, it performs better than any other 3D search method when using the benzoxazole (2f8i) template.

2D Selection from Multiple Templates with LigMatch. Given the considerable structural diversity among the TTR actives in the test set and the fact that these compounds explore different subregions of TTR pockets, we explored LigMatch’s multiple-template mode to assess the influence of adding extra layers of information in a single 3D search VS run.

Considerable improvements in terms of both early and overall enrichments are achieved when using the 2D selection from multiple templates and employing the strongest inhibitors of each of the three clusters as templates (PDB codes 1dvy, 2f8i, and 2g5u). In fact, the most remarkable increases are attained by inclusion of T₄ (2rox), the fourth template (see Figure 4 and Table 2).

This observation supports the notion that, although T₄ is neither a high-affinity binder nor a potent amyloid inhibitor, this endogenous TTR binder may hold specific features that are critical to the interaction with TTR and/or to better represent the chemical space of known TTR binders than other features presented by stronger inhibitors (whose binding may be merely more favorable entropically). To test this idea, we replaced the strong binder benzoxazole acid (compound **10**), which lacks some key substituent groups, by T₄ (compound **1**), in a third multiple-template scheme. A visible increase in both early and overall enrichment was obtained (see Figure 4), although more modest than that obtained with the four-template scheme (described above). In all cases and as pointed out in the LigMatch paper by Kinnings and Jackson,³⁶ ranking by the normalized mean score provides better results than ranking by the normalized best score.

Similarity Searches Using Concatamers. Another possible strategy to address the problem of low “representativeness” by single templates and to improve the performance of similarity searches would be to designate certain features as being essential, for example, the negatively charged carboxylates interacting with Lys-15 residues at the entrance of TTR pockets or the ionizable hydroxyl interacting with Ser-117 residues at the opposite end of the pockets. Conceptually, this would be equivalent to a 3D pharmacophore. Therefore we modeled four composite templates,

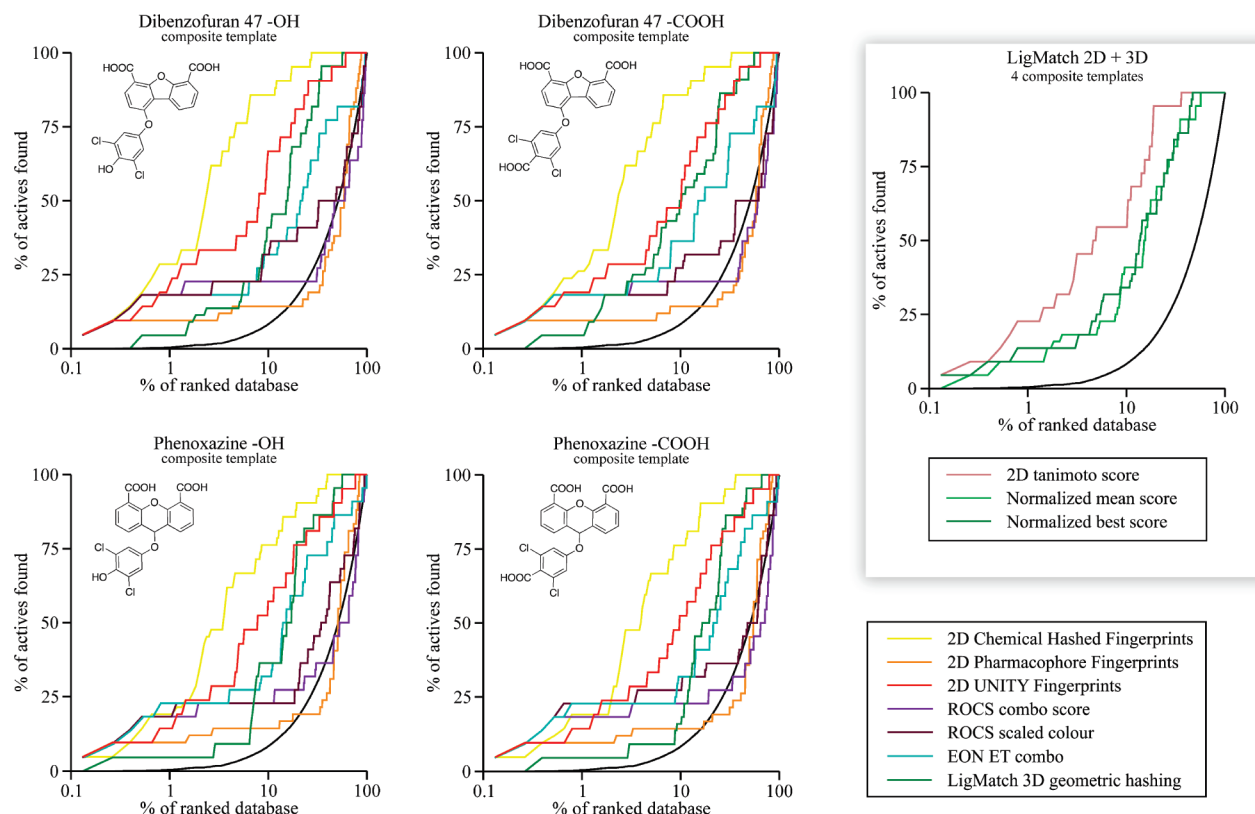


Figure 5. ROC curves to compare the performance of different VS protocols using four different composite ligands as single templates (panels in the left and center). The lines are colored as follows: 2D CHFs in yellow, 2D-PFs in orange, 2D UNITY fingerprints in red, ROCS combo score in indigo, ROCS scaled color in maroon, EON ET combo in turquoise, and the single-template mode of LigMatch in dark green. The use of a 2D selection from the four composite ligands, as implemented in LigMatch's multiple-template mode, is also compared with the single-template mode (panel in the right), using normalized best (in dark green) and mean (in green) scores and a 2D Tanimoto score (in brown) for ranking.

by adding a few features believed to be essential to strong reference templates, and tested them using all similarity search methods available. The results are shown in Figure 5 and Table 3.

In spite of their very close similarity, the two families of concatamers provide slightly different results in terms of early and overall enrichment. The templates derived from the DBF47 (inhibitor **5c**) yield the highest enrichment profiles of the whole benchmark with the CHF method (and the Euclidean distance metric). Indeed, ROCE values of 142.5, 42.2, and 26.2 respectively at 1, 2, and 5% of the ranked test set, along with an AUC of 0.95, are obtained with the DBF47-OH template (compound **24**), which are quite impressive results. Conversely, significant improvement to 3D similarity searches is only obtained with the phenox-derived templates. In particular, the phenox-OH template (compound **26**) positively influences the results of EON, yielding the highest early enrichment at 1% achieved with a 3D similarity search protocol and an acceptable overall enrichment. These results are only comparable with those obtained with the PCB18 and the phenox templates.

With an average AUC of 0.82 across the four concatamers, the geometric hashing procedure of LigMatch provides the best overall enrichment of all the 3D methods. However, poor early enrichments are generally obtained using single templates, contrasting with the results achieved using the 2D selection procedure from the more diverse templates (as also seen in the previous subsection). To study the influence of these two factors (i.e., the 2D selection step and the diversity

among the template molecules), we reranked the test set using the multiple-template protocol with 2D selection from the four concatamers. Although a considerable improvement in early enrichment is observed, the values are still far below those obtained using the four templates 1dvy, 2f8i, 2g5u, and 2rox (see last row in Table 2). These results confirm that, unlike the single-template similarity search methods tested, LigMatch (particularly its single-template mode) does not benefit from the use of the composite templates.

Docking and Scoring: Structure-Based Virtual Screening. In this study we evaluated the performance of 4 docking algorithms and 9 different scoring functions at predicting the native pose of TTR binders in 24 X-ray complexes (further information is provided in the Supporting Information). ROCE curves resulting from the scoring of docking poses generated by AD4 for the test set are provided in Figure 6. For comparison, we also provide the results obtained by scoring docked poses generated by FRED with ChemGauss3 and ChemScore functions. The visual analysis of the curves shows that in general the enrichments are poor and only slightly better than random selection. Surprisingly, even though FRED performs weakly at pose prediction, it provides better early and overall enrichment than AD4 (see Table 4). This is an interesting realization, since FRED is the fastest algorithm tested and, hence, the most suitable for ultrahigh-throughput docking. The best enrichments, however, are obtained by rescoring ligand poses generated by AD4 with DrugScore-CSD (ROCE values of 23.7, 13.6, and 7.9 at the top-scored 1, 2, and 5% of the ranked test set,

Table 3. ROCE Values at 0.5, 1, 2, and 5% and AUC Values of ROC Plots for Four Composite Templates Using Different Methods on TTR^a

original template/key R-group added/method		enrichment				ROCE AUC	
		0.5% ^b	1%	2%	10%		
DBF47	OH	2D CHF Euclidean	max.	142.5	42.2	26.2	0.95
		2D PF Tanimoto	47.5	11.9	5.6	3.0	0.50
		2D UNITY Tanimoto	142.0	59.5	33.3	9.5	0.87
		ROCS combo score	max.	36.2	17.5	5.2	0.47
		ROCS scaled color	max.	36.2	12.9	5.2	0.57
		EON ET_combo	max.	36.2	12.9	4.0	0.69
		LigMatch STM	11.3	5.0	6.9	2.9	0.83
phenox	COOH	2D CHF Euclidean	max.	101.0	42.2	23.0	0.95
		2D PF Tanimoto	47.5	11.9	5.6	2.0	0.49
		2D UNITY Tanimoto	142.0	38.0	23.8	9.5	0.86
		ROCS combo score	max.	36.2	12.9	5.2	0.45
		ROCS scaled color	max.	36.2	12.9	4.0	0.53
		EON ET_combo	max.	36.2	22.7	9.1	0.69
		LigMatch STM	11.3	5.0	12.9	6.3	0.84
all 4 concatamers	OH	2D CHF Euclidean	142.0	38.0	33.3	20.8	0.92
		2D PF Tanimoto	47.5	11.9	7.2	3.0	0.52
		2D UNITY Tanimoto	47.5	23.7	18.3	11.0	0.84
		ROCS combo score	max.	36.2	17.5	5.2	0.51
		ROCS scaled color	max.	36.2	17.5	5.2	0.60
		EON ET_combo	max.	113.5	17.5	6.3	0.75
		LigMatch STM	11.3	5.0	2.5	1.9	0.82
phenox	COOH	2D CHF Euclidean	94.8	38.0	18.3	20.8	0.93
		2D PF Tanimoto	47.5	11.9	5.6	3.0	0.51
		2D UNITY Tanimoto	47.5	23.7	18.3	7.9	0.83
		ROCS combo score	max.	36.2	12.9	5.2	0.45
		ROCS scaled color	max.	56.8	17.5	6.3	0.56
		EON ET_combo	max.	56.8	17.5	5.2	0.75
		LigMatch STM	11.3	5.0	2.5	1.9	0.79
all 4 concatamers		LigMatch multiple-template mode	45.0	11.3	10.7	3.9	0.82

^a The best combinations of method and template are identified in bold. ^b This percentage of the ranked test set of 760 ligands corresponds to only 4 ligands. When these top-score ligands are all actives, the ROCE value becomes the result of a division by zero. Accordingly, the result is presented as “max.”

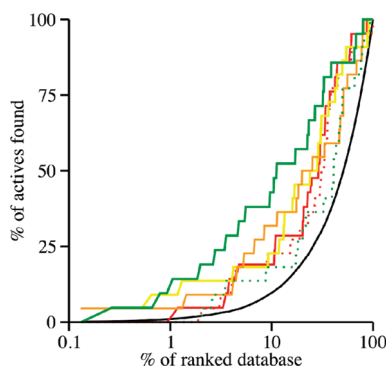


Figure 6. ROC curves to compare the VS performance of six docking and scoring schemes on a test set created for TTR. The lines are colored as follows: AD4 with its free energy function, versions 4.22 and version 4.01 (red straight and dotted lines, respectively); FRED with ChemGauss3 and ChemScore (yellow and orange straight lines, respectively); AD4 + DrugScore-CSD and + DrugScore-PDB (green straight and dotted lines, respectively).

respectively). These numbers are encouraging for docking and scoring methods, although the enrichment values are lower than those obtained with most ligand-based methods (as shown in previous subsections).

Another compelling result obtained with DrugScore-CSD was the assignment of inhibitor **22** (PCB18) with the highest

score of the test set. This compound has been reported as the most potent TTR amyloid inhibitor discovered.²⁰ Moreover, its molecular weight of only 322 Daltons is fairly lower than that of some of the most important inhibitors, such as phenox, DBF47, or bisaryloxime-5F (413, 415, and 466 Da, respectively), which is suggestive of a low influence of molecular weight on the scoring by DrugScore-CSD. We confirmed this supposition by plotting the scores assigned to each compound in our diverse set of decoys against its respective molecular weight. AD4 scores exhibit a considerable dependence on molecular weight, with a Pearson correlation coefficient of -0.40, whereas DrugScore-CSD displays an only marginal dependence, with a positive correlation of 0.11 (see Figure SI5, Supporting Information).

Pilot VS Campaign: Inspection of Screening Hits. To survey the potential of the VS protocols to retrieve promising new leads, we used the best-performing similarity search methods and templates (identified in bold across Tables 1–3) to rank a screening set of approximately 2.3 million compounds (described in the Methods Section). Given the high speed of FRED, the library was also docked and ranked using its built-in ChemGauss3 and ChemScore scoring functions (identified in bold in Table 4). Next, to ascertain the complementarity between protocols we examined the degree of overlap among the top 1000 hits retrieved by each protocol (a heat map is provided in Figure SI6, Supporting Informa-

Table 4. ROCE Values at 0.5, 1, 2, and 5% and AUC Values of ROC plots for Docking and Scoring Methods Tested on TTR

method/scoring function	ROC enrichment					ROCE AUC
	0.5%	1%	2%	5%		
AutoDock4 ^a	free energy func. 4.01	0	0	1.3	3.9	0.67
	free energy func. 4.22	0	2.6	2.6	4.1	0.70
FRED ^b	ChemGauss3	11.3	11.3	8.5	4.0	0.71
	ChemScore	11.3	5.0	5.3	4.0	0.67
AutoDock4 + DrugScore ^a	DrugScore-CSD	11.8	23.7	13.6	7.9	0.78
	DrugScore-PDB	0	0	0	2.9	0.60

^a The best docking and scoring results for this method were obtained with TTR structure of PDB code 1bm7. ^b The best docking and scoring results for this method were obtained with TTR structure with PDB code 2g9k.

tion). As anticipated, given the large size of the screening set and the diversity of methods employed, a high level of complementarity is found across the VS protocols, with approximately 80% of the hits being unique. As also expected, the patterns of overlap are consistent with commonalities in the underlying VS protocols. Indeed, protocols employing the same template query and/or similarity metric consistently show some overlap. The highest degree of overlap is observed among 2D similarity search methods employing the same similarity metric. However, 2D-PF represent an interesting outlier, showing a pattern of overlap similar to that of ROCS combo score, LigMatch, and docking with FRED (i.e., no significant overlap with any other method). These results prove that the use of 2D fingerprints alone is associated with a more conservative selection, strongly biased toward the chosen template. The increase in complexity of the methods by inclusion of additional information, such as molecular shape, electrostatic properties, multiple templates, or receptor structure data, yields a more distinctive selection of compounds, which is a sought outcome for a VS campaign.

Given the undesirable features associated with many TTR amyloid inhibitors identified to date, the screening of new lead compounds with diverse properties is a critical goal. At this stage we are particularly interested in selecting potential inhibitors with adequate solubility profiles, low propensity for aggregation, and reduced halide fraction. Figure 7 summarizes predicted physicochemical properties for the top 100 hits retrieved by each of the best-performing VS protocols. Additional information is given in Table SI2, Supporting Information. It is worth noting that despite the use of template queries holding heavy halogen atoms, the median values for molecular weight across all sets of hits is within the range of lead-likeness, typically defined between 150 and 440 Da. This may relate back to the low halide fraction of our tailored screening set, translated into low halide fractions among the top hits (null median halide fraction for most VS protocols). However, there are at least two noticeable exceptions to this trend (see Figure 7, VS protocols 2Dsim CHF Tanimoto PCB18 and 2D UNITY Tanimoto PCB18) and a few outliers among the VS hits with near-maximum halide fraction allowance (e.g., see Figure 7, ROCS scaled color T₄), which shows that the chosen VS protocols can themselves suggest molecules devoid of undesirable halogens. Alongside this, the predicted octanol/water partition coefficients ($X \log P$) and solubility profiles of the selected hits are by far more favorable than those of the known actives. Eighteen out of the 26 known actives (69%) fall in the insoluble, poorly, or moderately soluble

categories, whereas only 234 out of 1900 top hits (12%) fit in these categories. Moreover, 31% of the known actives are predicted aggregators, whereas only 0.7% of the retrieved hits fail the aggregator filter. Interestingly, VS protocols employing T₄ as a template query (namely VS protocols 2D CHF Euclidean T₄, ROCS scaled color T₄, and LigMatch) retrieve the most soluble series of candidates.

From the pharmacological viewpoint, targeting TTR represents an uncharacteristic challenge, since the blood plasma constitutes not a vessel for drug distribution but the actual target compartment itself. Therefore, an important aspect to take into consideration during the selection/design of inhibitors is their ability to cross membranes and spread through compartments where they are likely to cause adverse effects. The polar surface area (PSA) is a descriptor that has shown good inverse correlation with passive transport across biological membranes. A PSA of 60 Å² or less is associated with the ability to permeate the blood–brain barrier, whereas 140 Å² is the higher limit for drug absorption. Kelder et al. suggested a “window of opportunity” for designing non-CNS penetrating and orally absorbed compounds, by maintaining PSA values between 70 and 120 Å².⁷⁰ The median PSA value for the known TTR actives is 60 Å². In contrast, most of the series of hits present a median PSA value superior to 70 Å². The exceptions are mostly comprised of the series selected by 2D similarity searches using PCB18 as template. At this point it should be noted that although PCB18 is a highly potent inhibitor of TTR amyloid, it is part of a family of compounds (PCBs) that has been connected with bioaccumulation, rodent and human toxicity (see ref 16 and references therein). These features can be linked with the high hydrophobicity of the compounds or their low PSA. Even though PCB18 has proved to be a successful template in terms of VS performance (see previous subsections), a critical analysis of hits retrieved by VS protocols employing this template must be undertaken.

All series of top 100 hits were docked to the binding sites of TTR with AD4, along with all active, composite, and decoy molecules. The resulting complexes were visually inspected and rescored with DrugScore-CSD. Detailed results are given in the Supporting Information. In spite of the limited accuracy of scoring functions at predicting reported binding affinities, DrugScore-CSD is able to distinguish reasonably well the known TTR actives from the decoy molecules (as seen in the enrichment studies). In general, interactions established with the known actives on pocket AC are assigned with better scores than interactions within pocket BD. Although no consistent structural differences were found between the two binding sites across multiple

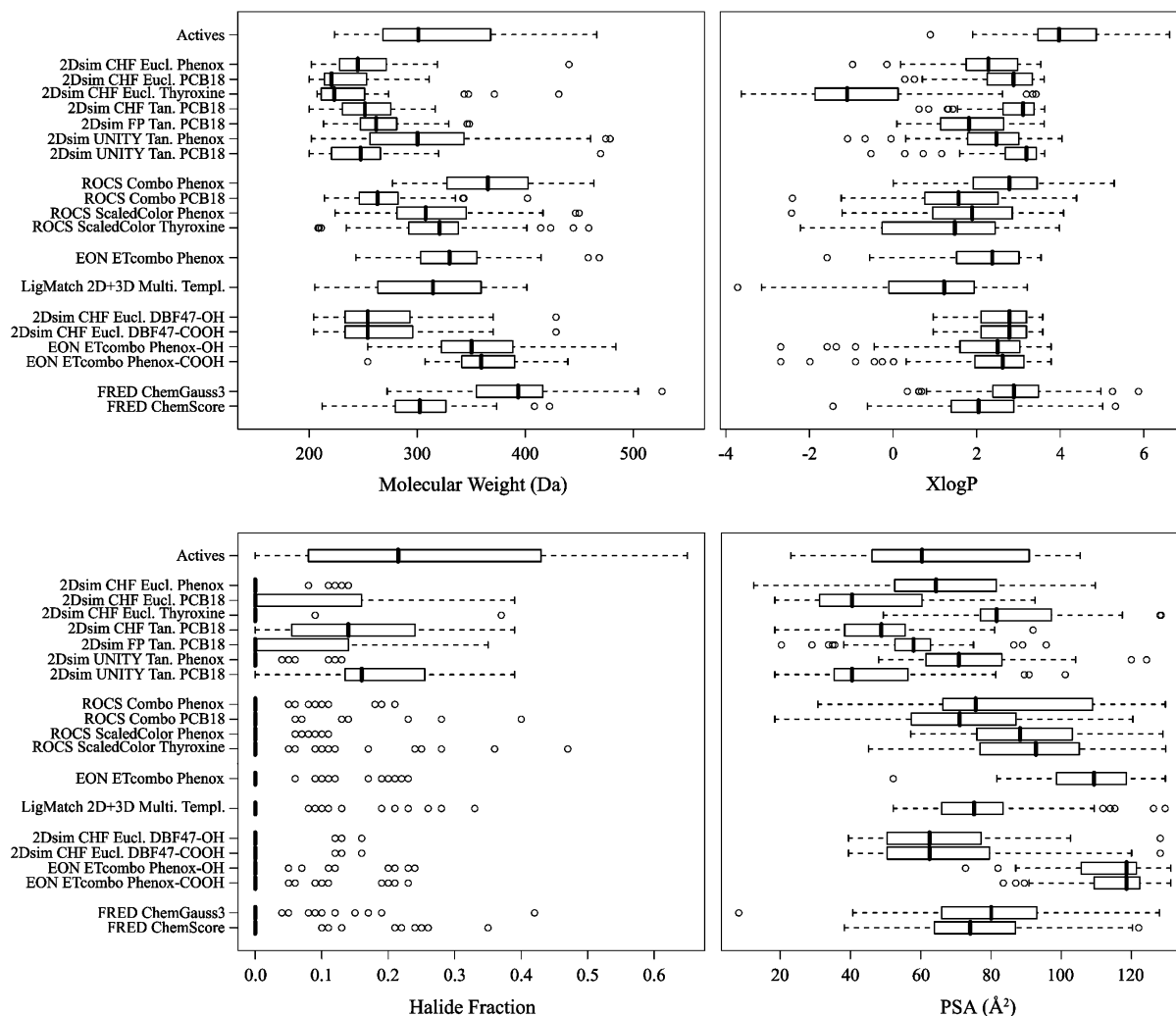


Figure 7. Box plots (box region providing a graphical view of the median and quartiles of the distribution; dotted lines extending to maximum and minimum values of the data set) to compare four different physicochemical properties across the top 100 hit compounds retrieved by each VS protocol. The properties of TTR actives (compounds 1–23 in Figure 2) are given in the first row for comparison purposes.

complexes, the number of hydrogen bonds established with the TTR receptor is consistently inferior on pocket BD for all ligand series. This result might be related with the negative cooperativity effects experimentally observed for most TTR binders. The median score attained for the active compounds on pocket AC is the highest of all series. This does not apply to pocket BD, however, where the median scores favor some of the series of VS hits, namely those retrieved using the 2D UNITY phenox, LigMatch, 2D CHF DBF47 COOH and FRED ChemScore protocols. Better combinations of median scores on the two TTR pockets are in fact found for many VS hit series, which might be a good indication for potential candidates with favorable binding cooperativity.

Furthermore, the compliance of the VS hits with the pharmacophore hypotheses devised for both TTR pockets was assessed by running UNITY 3D pharmacophore searches. Not surprisingly, VS protocols employing phenox as a template were able to identify ligands that fit the more specific HYP AC1 (see Figure 1D). On the other hand, protocols using the PCB18 template performed better at retrieving ligands that fit the more general (and “promiscuous”) pharmacophores for TTR, such as HYP BD1 (Figure

1D) and mainly HYP AC2 and HYP BD2 (Figures S1 and S2, Supporting Information). While the latter models may be useful to identify a higher number of TTR binders, HYP AC1 seems to show promise for identifying more specific inhibitors. Combinations of hypotheses will be used for postprocessing hits retrieved by a large-scale VS campaign currently running on the Ibercivis volunteer computing network⁷¹ and thus prioritizing candidates for experimental evaluation.

CONCLUSIONS

In this work we present a comparative evaluation of different virtual screening approaches for identifying new transthyretin (TTR) stabilizer compounds to inhibit amyloid fibril formation. Using a test set comprising the most important stabilizers discovered to date and carefully selected decoy molecules, we compare the performance of several methods employing two-dimensional (2D) descriptors, 3D similarity searches, and molecular docking. Furthermore, two sets of pharmacophore models characterizing the determinants of ligand binding to each pocket are presented on the basis of the differential positioning

of the ligands in the pockets. The performance of the different methods and models is assessed using enrichments of the known actives within the top-scored compounds. By combining the best-performing virtual screening (VS) protocols, a subset of small molecules was retrieved from a tailored library of 2.3 million commercially available compounds. This subset was analyzed and shows distinctive features from the known stabilizers, holding better physicochemical properties and combined affinity for both TTR pockets according to our predictions.

Focusing only on the enrichment profiles obtained, the ligand-based methods performed better than the protein-based methods (i.e., docking into TTR structures). In particular, 2D similarity search methods were able to offer the best discrimination between the known TTR actives and the decoy molecules. Given the reasonable structural diversity found among the known actives, these methods provide a good balance between both search specificity, a key aspect for target selectivity, and flexibility, which is necessary for eliminating the dependency on the used templates. In fact, the top VS hits returned by these methods show the highest compliance with the pharmacophore models devised for TTR. However, their structural similarity to the employed templates is obvious, disclosing limited scaffold hopping capabilities for 2D similarity search methods. While producing worst enrichments than 2D methods, 3D similarity search methods based on shape and chemical complementarity were able to suggest novel scaffolds with noticeable added value when electrostatic similarity was included as a descriptor. Yet, because these methods use one single bioactive template molecule they often overlook strong TTR stabilizers with dissimilar structure. The use of concatamers to address the problem of representativeness of single templates brings improvement to the performance of similarity search methods, and even more balanced outcomes are attained with LigMatch, a method that can employ multiple templates and combine 3D geometric hashing with a 2D preselection process.

Efforts made in the field of docking and scoring are noteworthy, but our results highlight limitations of scoring functions in common use when handling nonspecific binders with hydrophobic pockets, such as TTR. However, we have successfully identified a combination of a docking (AD4) and scoring (DrugScore-CSD) method that is able to provide encouraging enrichment profiles for TTR and negligible bias toward the molecular weight of the ligands. This combination was used along with 3D pharmacophore models to prioritize the most promising candidates among the top VS hits retrieved by fast ligand-based similarity search protocols and by a fast rigid docking algorithm (FRED). By analysis of the median and maximum score values obtained with DrugScore-CSD for the top VS hits, we detect balanced profiles for the estimated binding affinities on the two pockets of TTR and a good agreement between the fast docking protocols and the best-performing docking and scoring combination. Nevertheless, when compared with the high-scoring compounds retrieved by most ligand-based methods, a larger percentage of potential false positives (compounds with inappropriate molecular shape, size, or chemical topology) is found among the hits retrieved by docking methods.

To sum up, we emphasize the importance of a thorough validation of VS methods as an essential step to a VS campaign against any target of biological relevance. It should be noted that this study cannot provide an exhaustive comparison of all VS techniques currently available, and different or better results could have been obtained using other methods. The increase in complexity of the VS protocols by inclusion and combination of additional layers of information (such as molecular shape, electrostatic properties, the use of composite or multiple templates, and receptor information in molecular docking) may be accompanied by decreases in performance on a given test set, yet increase the likelihood of retrieving new and promising scaffolds with distinctive physicochemical properties. Of critical relevance to the work presented here are the exceptional solubility, appropriate polar surface areas, and low halogen fraction characterizing the series of compounds identified on a preliminary VS campaign for TTR amyloid inhibitors. Further validation of the tested protocols will be carried out through the experimental evaluation of selected compounds for their ability to bind TTR and prevent fibril formation *in vitro*. Lessons learned in this work are currently being applied in a large-scale VS campaign conducted by our group on the Ibercivis platform and can be broadly employed toward the identification of novel and safer TTR amyloid inhibitors.

ACKNOWLEDGMENT

The authors thank Fundação para a Ciência e a Tecnologia (FCT) and the program FEDER for financial support through project PTDC/BIA-PRO/72838/2006. Acknowledgments are also due to the Center for Computational Physics, Departamento de Física, Universidade de Coimbra, Coimbra, Portugal and the Computer Science and Technology Center, Departamento de Informática, Universidade do Minho, Braga, Portugal for the computer resources provided. C.J.V.S. thanks FCT for a Ph.D grant SFRH/BD/29357/2006.

Supporting Information Available: Description of 3D pharmacophore models and their evaluation, validation of docking and scoring programs at ligand pose prediction, and results from a pilot virtual screening campaign. This material is available free of charge via the Internet at <http://pubs.acs.org>.

REFERENCES AND NOTES

- (1) De Lorenzi, E.; Giorgetti, S.; Grossi, S.; Merlini, G.; Caccialanza, G.; Bellotti, V. Pharmaceutical Strategies Against Amyloidosis: Old and New Drugs in Targeting a Protein Misfolding Disease. *Curr. Med. Chem.* **2004**, *11*, 1065–1084.
- (2) Quintas, A.; Vaz, D. C.; Cardoso, I.; Saraiva, M. J.; Brito, R. M. Tetramer Dissociation and Monomer Partial Unfolding Precedes Prototubular Formation in Amyloidogenic Transthyretin Variants. *J. Biol. Chem.* **2001**, *276*, 27202–27213.
- (3) Brito, R. M.; Damas, A. M.; Saraiva, M. J. Amyloid Formation by Transthyretin: From Protein Stability to Protein Aggregation. *Curr. Med. Chem.: Immunol., Endocr. Metab. Agents* **2003**, *3*, 349–360.
- (4) Mirov, G. J.; Lai, Z.; Lashuel, H. A.; Peterson, S. A.; Strang, C.; Kelly, J. W. Inhibiting Transthyretin Amyloid Fibril Formation Via Protein Stabilization. *Proc. Natl. Acad. Sci. U.S.A.* **1996**, *93*, 15051–15056.
- (5) Hammarström, P.; Jiang, X.; Hurshman, A. R.; Powers, E. T.; Kelly, J. W. Sequence-Dependent Denaturation Energetics: A Major Determinant in Amyloid Disease Diversity. *Proc. Natl. Acad. Sci. U.S.A.* **2002**, *99* (Suppl 4), 16427–16432.
- (6) Hurshman, A. R.; White, J. T.; Powers, E. T.; Kelly, J. W. Transthyretin Aggregation Under Partially Denaturing Conditions Is A Downhill Polymerization. *Biochemistry* **2004**, *43*, 7365–7381.

- (7) Wiseman, R. L.; Johnson, S. M.; Kelker, M. S.; Foss, T.; Wilson, I. A.; Kelly, J. W. Kinetic Stabilization of an Oligomeric Protein by a Single Ligand Binding Event. *J. Am. Chem. Soc.* **2005**, *127*, 5540–5551.
- (8) Munro, S. L.; Lim, C. F.; Hall, J. G.; Barlow, J. W.; Craik, D. J.; Topliss, D. J.; Stockigt, J. R. Drug Competition for Thyroxine Binding to Transthyretin (Prealbumin): Comparison with Effects on Thyroxine-Binding Globulin. *J. Clin. Endocrinol. Metab.* **1989**, *68*, 1141–1147.
- (9) Baures, P. W.; Peterson, S. A.; Kelly, J. W. Discovering Transthyretin Amyloid Fibril Inhibitors by Limited Screening. *Bioorg. Med. Chem.* **1998**, *6*, 1389–1401.
- (10) Baures, P. W.; Oza, V. B.; Peterson, S. A.; Kelly, J. W. Synthesis and Evaluation of Inhibitors of Transthyretin Amyloid Formation Based on the Non-Steroidal Anti-Inflammatory Drug, Flufenamic Acid. *Bioorg. Med. Chem.* **1999**, *7*, 1339–1347.
- (11) Oza, V. B.; Petrassi, H. M.; Purkey, H. E.; Kelly, J. W. Synthesis and Evaluation of Anthranilic Acid-Based Transthyretin Amyloid Fibril Inhibitors. *Bioorg. Med. Chem.* **1999**, *9*, 1–6.
- (12) Klabunde, T.; Petrassi, H. M.; Oza, V. B.; Raman, P.; Kelly, J. W.; Sacchettini, J. C. Rational Design of Potent Human Transthyretin Amyloid Disease. *Nat. Struct. Biol.* **2000**, *7*, 312–321.
- (13) Oza, V. B.; Smith, C.; Raman, P.; Koepf, E. K.; Lashuel, H. A.; Petrassi, H. M.; Chiang, K. P.; Powers, E. T.; Sacchettini, J.; Kelly, J. W. Synthesis, Structure, and Activity of Diclofenac Analogues as Transthyretin Amyloid Fibril Formation Inhibitors. *J. Med. Chem.* **2002**, *45*, 321–332.
- (14) Hammarström, P.; Wiseman, R. L.; Powers, E. T.; Kelly, J. W. Prevention of Transthyretin Amyloid Disease by Changing Protein Misfolding Energetics. *Science* **2003**, *299*, 713–716.
- (15) Powers, E. T.; Wiseman, R. L.; Purkey, H. E. Benzoxazoles as Transthyretin Amyloid Fibril Inhibitors: Synthesis, Evaluation, and Mechanism of Action. *Angew. Chem., Int. Ed.* **2003**, *42*, 2758–2761.
- (16) Purkey, H. E.; Palaninathan, S. K.; Kent, K. C.; Smith, C.; Safe, S. H.; Sacchettini, J. C.; Kelly, J. W. Hydroxylated Polychlorinated Biphenyls Selectively Bind Transthyretin in Blood and Inhibit Amyloidogenesis: Rationalizing Rodent PCB Toxicity. *Chem. Biol.* **2004**, *11*, 1719–1728.
- (17) Adamski-Werner, S. L.; Palaninathan, S. K.; Sacchettini, J. C.; Kelly, J. W. Diflunisal Analogs Stabilize the Native State of Transthyretin. Potent Inhibition of Amyloidogenesis. *J. Med. Chem.* **2004**, *47*, 355–374.
- (18) Johnson, S. M.; Petrassi, H. M.; Palaninathan, S. K.; Mohamedmo-haideen, N. N.; Purkey, H. E.; Nichols, C.; Chiang, K. P.; Walkup, T.; Sacchettini, J. C.; Sharpless, K. B.; Kelly, J. W. Bisaryloxime Ethers as Potent Inhibitors of Transthyretin Amyloid Fibril Formation. *J. Med. Chem.* **2005**, *48*, 1576–1587.
- (19) Petrassi, H. M.; Johnson, S. M.; Purkey, H.; Chiang, K. P.; Walkup, T.; Jiang, X.; Powers, E. T.; Kelly, J. W. Potent and Selective Structure-Based Dibenzo[furan] Inhibitors of Transthyretin Amyloidogenesis: Kinetic Stabilization of the Native State. *J. Am. Chem. Soc.* **2005**, *127*, 6662–6671.
- (20) Johnson, S. M.; Connelly, S.; Wilson, I. A.; Kelly, J. W. Biochemical and Structural Evaluation of Highly Selective 2-Arylbenzoxazole-Based Transthyretin Amyloidogenesis Inhibitors. *J. Med. Chem.* **2008**, *51*, 260–270.
- (21) Choi, S.; Reixach, N.; Connelly, S.; Johnson, S. M.; Wilson, I. A.; Kelly, J. W. A Substructure Combination Strategy to Create Potent and Selective Transthyretin Kinetic Stabilizers That Prevent Amyloidogenesis and Cytotoxicity. *J. Am. Chem. Soc.* **2010**, *132*, 1359–1370.
- (22) Johnson, S. M.; Connelly, S.; Wilson, I. A.; Kelly, J. W. Toward Optimization of the Second Aryl Substructure Common to Transthyretin Amyloidogenesis Inhibitors Using Biochemical and Structural Studies. *J. Med. Chem.* **2009**, *52*, 1115–1125.
- (23) Choi, S.; Connelly, S.; Wilson, I. A.; Kelly, J. W. Chemoselective Small Molecules That Covalently Modify One Lysine in a Non-Enzyme Protein in Plasma. *Nat. Chem. Biol.* **2010**, *6*, 133–139.
- (24) Buxbaum, J. N.; Reixach, N. Transthyretin: the Servant of Many Masters. *Cell. Mol. Life Sci.* **2009**, *66*, 3095–3101.
- (25) Warren, G. L.; Andrews, C. W.; Capelli, A.; Clarke, B.; LaLonde, J.; Lambert, M. H.; Lindvall, M.; Nevins, N.; Semus, S. F.; Senger, S.; Tedesco, G.; Wall, I. D.; Woolven, J. M.; Peishoff, C. E.; Head, M. S. A Critical Assessment of Docking Programs and Scoring Functions. *J. Med. Chem.* **2006**, *49*, 5912–5931.
- (26) Willett, P. Similarity-Based Virtual Screening Using 2D Fingerprints. *Drug Discovery Today* **2006**, *11*, 1046–1053.
- (27) Eckert, H.; Bajorath, J. Design and Evaluation of A Novel Class-Directed 2D Fingerprint to Search for Structurally Diverse Active Compounds. *J. Chem. Inf. Model.* **2006**, *46*, 2515–2526.
- (28) Rush, T. S.; Grant, J. A.; Mosyak, L.; Nicholls, A. A Shape-Based 3-D Scaffold Hopping Method and Its Application to a Bacterial Protein-Protein Interaction. *J. Med. Chem.* **2005**, *48*, 1489–1495.
- (29) Doddareddy, M. R.; Choo, H.; Cho, Y. S.; Rhim, H.; Koh, H. Y.; Lee, J.; Jeong, S.; Pae, A. N. 3D Pharmacophore Based Virtual Screening of T-Type Calcium Channel Blockers. *Bioorg. Med. Chem.* **2007**, *15*, 1091–1105.
- (30) Evers, A.; Hessler, G.; Matter, H.; Klabunde, T. Virtual Screening of Biogenic Amine-Binding G-Protein Coupled Receptors: Comparative Evaluation of Protein- and Ligand-Based Virtual Screening Protocols. *J. Med. Chem.* **2005**, *48*, 5448–65.
- (31) Iraee, G.; Edelhoch, H. Thyroxine-Induced Conformational Changes in Prealbumin. *Biochemistry* **1978**, *17*, 5729–5733.
- (32) JChem 5.1.4, 2008, ChemAxon (www.chemaxon.com).
- (33) SYBYL 7.3, 2006, Tripos International: St. Louis, MO.
- (34) ROCS, version 2.3.1, 2007, Openeye Scientific Software, Inc: Santa Fe, NM.
- (35) EON, version 2.0.1, 2007, Openeye Scientific Software, Inc: Santa Fe, NM.
- (36) Kinnings, S. L.; Jackson, R. M. LigMatch: A Multiple Structure-Based Ligand Matching Method for 3D Virtual Screening. *J. Chem. Inf. Model.* **2009**, *49*, 2056–2066.
- (37) Morris, G. M.; Goodsell, D. S.; Halliday, R. S.; Huey, R.; Hart, W. E.; Belew, R. K.; Olson, A. J. Automated Docking Using a Lamarckian Genetic Algorithm and An Empirical Binding Free Energy Function. *J. Comput. Chem.* **1998**, *19*, 1639–1662.
- (38) McGann, M. R.; Almond, H. R.; Nicholls, A.; Grant, J. A.; Brown, F. K. Gaussian Docking Functions. *Biopolymers* **2003**, *68*, 76–90.
- (39) Vriend, G. WHAT IF: A Molecular Modeling and Drug Design program. *J. Mol. Graph.* **1990**, *8* (52–6), 29.
- (40) Laskowski, R. A.; MacArthur, M. W.; Moss, D. S.; Thornton, J. M. PROCHECK - A Program to Check the Stereochemical Quality of Protein Structures. *J. Appl. Crystallogr.* **1993**, *26*, 283–291.
- (41) Henrick, K.; Thornton, J. M. PQS: a protein quaternary structure file server. *Trends Biochem. Sci.* **1998**, *23*, 358–361.
- (42) Brakoulias, A.; Jackson, R. M. Towards a Structural Classification of Phosphate Binding Sites in Protein-Nucleotide Complexes: An Automated All- Against-All Structural Comparison Using Geometric Matching. *Biochemistry* **2004**, *260*, 250–260.
- (43) Halgren, T. A. Merck Molecular Force Field: I. Basis, Form, Scope, Parameterization and Performance of MMFF94. *J. Comput. Chem.* **1996**, *17*, 490–519.
- (44) Zhao, Y.; Karypis, G. Data Clustering in Life Sciences. *Mol. Biotechnol.* **2005**, *31*, 055–080.
- (45) Huang, N.; Shoichet, B. K.; Irwin, J. J. Benchmarking Sets for Molecular Docking. *J. Med. Chem.* **2006**, *49*, 6789–6801.
- (46) Irwin, J. J.; Shoichet, B. K. ZINC - A Free Database of Commercially Available Compounds for Virtual Screening. *J. Chem. Inf. Model.* **2005**, *45*, 177–182.
- (47) FILTER, version 2.0.2, 2007, Openeye Scientific Software, Inc: Santa Fe, NM.
- (48) Lipinski, C. Experimental and Computational Approaches to Estimate Solubility and Permeability in Drug Discovery and Development Settings. *Adv. Drug Deliv. Rev.* **1997**, *23*, 3–25.
- (49) Mills, J. E.; Dean, P. M. Three-Dimensional Hydrogen-Bond Geometry and Probability Information from a Crystal Survey. *J. Comput.-Aided Mol. Des.* **1996**, *10*, 607–622.
- (50) Veber, D. F.; Johnson, S. R.; Cheng, H.; Smith, B. R.; Ward, K. W.; Kopple, K. D. Molecular Properties That Influence the Oral Bioavailability of Drug Candidates. *J. Med. Chem.* **2002**, *45*, 2615–2623.
- (51) Martin, Y. C. A bioavailability score. *J. Med. Chem.* **2005**, *48*, 3164–3170.
- (52) Egan, W. J.; Merz, K. M.; Baldwin, J. J. Prediction of Drug Absorption Using Multivariate Statistics. *J. Med. Chem.* **2000**, *43*, 3867–3877.
- (53) McGovern, S. L.; Helfand, B. T.; Feng, B.; Shoichet, B. K. A Specific Mechanism of Nonspecific Inhibition. *J. Med. Chem.* **2003**, *46*, 4265–4272.
- (54) Seidler, J.; McGovern, S. L.; Doman, T. N.; Shoichet, B. K. Identification and Prediction of Promiscuous Aggregating Inhibitors Among Known Drugs. *J. Med. Chem.* **2003**, *46*, 4477–4486.
- (55) OMEGA, version 2.2.1, 2008, Openeye Scientific Software, Inc: Santa Fe, NM.
- (56) Boström, J.; Greenwood, J. R.; Gottfries, J. Assessing the Performance of OMEGA with Respect to Retrieving Bioactive Conformations. *J. Mol. Graphics Modell.* **2003**, *21*, 449–462.
- (57) Kirchmair, J.; Distinto, S.; Markt, P.; Schuster, D.; Spitzer, G. M.; Liedl, K. R.; Wolber, G. How To Optimize Shape-Based Virtual Screening: Choosing the Right Query and Including Chemical Information. *J. Chem. Inf. Model.* **2009**, *49*, 678–692.
- (58) Wojtczak, A.; Cody, V.; Luft, J. R.; Pangborn, W. Structures of Human Transthyretin Complexed with Thyroxine at 2.0 Å Resolution and 3',5'-Dinitro-N-Acetyl-L-Thyronine at 2.2 Å Resolution. *Acta Crystallogr., Sect. D: Biol. Crystallogr.* **1996**, *52*, 758–765.
- (59) Marvin, 5.1.4, 2008, ChemAxon (www.chemaxon.com).
- (60) Power, D. M.; Elias, N. P.; Richardson, S. J.; Mendes, J.; Soares, C. M.; Santos, C. R. Evolution of the Thyroid Hormone-Binding Protein, Transthyretin. *Gen. Comp. Endocrinol.* **2000**, *119*, 241–255.

- (61) Weiner, P. K.; Langridge, R.; Blaney, J. M.; Schaefer, R.; Kollman, P. A. Electrostatic Potential Molecular Surfaces. *Proc. Natl. Acad. Sci. U.S.A.* **1982**, *79*, 3754–3758.
- (62) Zsoldos, Z.; Reid, D.; Simon, A.; Sadjad, S. B.; Johnson, A. P. eHiTS: A New Fast, Exhaustive Flexible Ligand Docking System. *J. Mol. Graphics Modell.* **2007**, *26*, 198–212.
- (63) Jones, G.; Willett, P.; Glen, R. C.; Leach, A. R.; Taylor, R. Development and Validation of a Genetic Algorithm for Flexible Docking. *J. Mol. Biol.* **1997**, *267*, 727–748.
- (64) Eldridge, M. D.; Murray, C. W.; Auton, T. R.; Paolini, G. V.; Mee, R. P. Empirical Scoring Functions: I. The Development of A Fast Empirical Scoring Function to Estimate the Binding Affinity of Ligands in Receptor Complexes. *J. Comput.-Aided Mol. Des.* **1997**, *11*, 425–445.
- (65) Mooij, W. T.; Verdonk, M. L. General and Targeted Statistical Potentials for Protein-Ligand Interactions. *Proteins* **2005**, *61*, 272–287.
- (66) Verkhivker, G. M.; Bouzida, D.; Gehlhaar, D. K.; Rejto, P. A.; Arthurs, S.; Colson, A. B.; Freer, S. T.; Larson, V.; Luty, B. A.; Marrone, T.; Rose, P. W. Deciphering Common Failures in Molecular Docking of Ligand-Protein Complexes. *J. Comput.-Aided Mol. Des.* **2000**, *14*, 731–751.
- (67) Stahl, M.; Rarey, M. Detailed Analysis of Scoring Functions for Virtual Screening. *J. Med. Chem.* **2001**, *44*, 1035–1042.
- (68) Velec, H. F.; Gohlke, H.; Klebe, G. Knowledge-Based Scoring Function Derived from Small Molecule Crystal Data with Superior Recognition Rate of Near-Native Ligand Poses and Better Affinity Prediction. *J. Mol. Biol.* **2005**, *348*, 6296–6303.
- (69) Nicholls, A. What Do We Know and When Do We Know It. *J. Comput.-Aided Mol. Des.* **2008**, *22*, 239–255.
- (70) Kelder, J.; Grootenhuis, P. J.; Bayada, D. M.; Delbressine, L. P.; Ploemen, J. Polar Molecular Surface as a Dominating Determinant for Oral Absorption and Brain Penetration of Drugs. *Pharm. Res.* **1999**, *16*, 1514–1519.
- (71) Citizen Computing Platform Ibercivis: www.bercivis.net (accessed on 9/27/2010).

CI100250Z